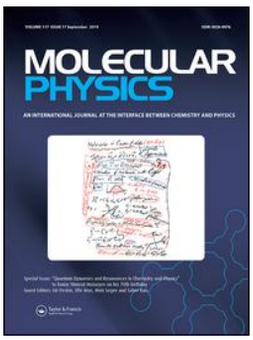

Molecular Physics

ISSN: 0026-8976 (Print) 1362-3028 (Online) Journal homepage: https://www.tandfonline.com/loi/tmph20

A unified description of MCl_3 systems with a polarizable ion simulation model

FRANCIS HUTCHINSON , MARK WILSON & PAUL A. MADDEN

To cite this article: FRANCIS HUTCHINSON , MARK WILSON & PAUL A. MADDEN (2001) A unified description of MCl_3 systems with a polarizable ion simulation model, Molecular Physics, 99:10, 811-824, DOI: 10.1080/00268970010022878

To link to this article: https://doi.org/10.1080/00268970010022878

Published online: 25 Nov 2009.

MOLECULAR PHYSICS, 2001, VOL. 99, NO. 10, 811–824

A unified description of MCl_3 systems with a polarizable ion simulation model

FRANCIS HUTCHINSON, MARK WILSON and PAUL A. MADDEN*
Physical and Theoretical Chemistry Laboratory, Oxford University, South Parks Road, Oxford OX1 3QZ, UK

(*Received 23 October 2000; revised version accepted 20 November 2000*)

Computer simulations of a range of ionic systems of stoichiometry MX_3 using a polarizable, formal charge ionic interaction model are described. The objective of the present work is to describe the optimization of the interaction potentials in the light of new structural information which has become available from neutron scattering studies of the liquid. As well as substantially improving the agreement with experiment for $LaCl_3$, $TbCl_3$, YCl_3 and $AlCl_3$, simulation results are presented for the first time for $ScCl_3$, which is shown to exhibit a fascinating cross-linked network structure. The optimization of potentials for the crystal structures is also considered. It is shown that the Cl^- ion must be considered as of smaller size in the crystal than in the liquid in order to successfully reproduce the properties of both phases.

1. Introduction

Substantial progress has been made in recent years in modelling the interactions in trivalent metal halides. As described below, these materials present an interesting challenge because their properties are not explicable on the basis of a simple ionic interaction [1–3]. Furthermore, the development of a reliable and transferable description of the interactions is highly desirable for technological reasons. A number of existing or proposed technologies, such as electrodeposition of refractory metals [4], or electrolytic separation of nuclear waste [5], involve solutions of trivalent metal halides in molten alkali halides. Since these processes often involve intense physical conditions (e.g. high T) or hazardous materials (e.g. actinides) which preclude detailed experimental characterization, it would be very valuable to be able to deduce key material properties, and to examine the processes in microscopic detail by computer simulation.

For many years, experimental information on the microstructure of these materials was very sparse. An exception is the area of Raman spectroscopy [6], where extensive measurements have been made, but the connection between the Raman observables and the actual atomic arrangement is not a direct one, and this obscures the relationship between the structure and the underlying interaction potential. Recently, neutron scattering measurements on a wide range of trivalent metal halides have been made and have provided data against which the structural predictions of computer simulation models can be tested and refined. Here we will present the results of such a refinement process, leading to a closely related family of potentials which reproduce the experimentally observed crystal structures and neutron diffraction derived liquid structures across the range from $LaCl_3$ to $AlCl_3$, involving all lanthanides, plus transition metal and main group trivalent cations with closed shell electronic structures. In the spirit of an extended ionic description of the interactions, the potentials are related simply through the cation radius, which determines the key parameters in a well defined way. For this reason potentials for other materials (e.g. actinides) should be predictable. Because the potentials reflect an underlying ionic picture of electronic structure (i.e. closed shell interactions and formal charges) they transfer well to ionic mixtures.

The lanthanide elements and a number of transition metal (Y, Sc) and main group elements (Al, etc.) form trivalent cations which systematically span a wide range of ionic radii. As the cation radius is reduced (from La to Al), the 'ionic' character of the melt decreases. $LaCl_3$ melts at a high temperature with a volume change ($\sim 16\%$) typical of ionic compounds, whereas $AlCl_3$ melts at a low temperature from an ionic crystal with an enormous ($\sim 80\%$) volume increase to form an insulating liquid, believed to be composed of Al_2Cl_6 dimers. Intermediate size cation systems, like $DyCl_3$ and YCl_3, are isomorphous with $AlCl_3$ in the crystal but melt to form network liquids, with a tiny volume increase on melting ($< 1\%$) in the case of YCl_3. Simulation studies

* Author for correspondence. e-mail: madden@physchem.ox.ac.uk

Molecular Physics ISSN 0026–8976 print/ISSN 1362–3028 online © 2001 Taylor & Francis Ltd
http://www.tandf.co.uk/journals
DOI: 10.1080/00268970010022878

with a 'generic' polarizable ionic potential for MCl_3 systems, in which the difference between different cations is expressed only through an ionic radius, recapture the major differences between the liquid structures, as witnessed by the recent neutron diffraction results. In particular, we have been able to recapture the molecular nature [7] of liquid $AlCl_3$ and obtain neutron and X-ray diffraction predictions which agree well with experiment for it and the slightly larger cation system $FeCl_3$ [8–10]. Akdeniz, Tosi and coworkers [11] have also discussed the stability of the Al_2Cl_6 molecule with a polarizable ionic potential model. We have achieved good comparisons [12] with the total neutron scattering data [13–18] for a number of larger cation systems (including $LaCl_3$ and $CeCl_3$), and demonstrated the importance of polarization effects in comparisons of the predicted structures with the resolved partial structure factors in molten $DyCl_3$ [19].

Nevertheless, detailed comparisons of the simulation predictions, with this generic potential across the full range of MCl_3 systems revealed a number of shortcomings [20]. Notably, the potentials failed to predict the ground state crystal structures correctly, although they did account for a dependence in the relative stability of the different possible crystal structures on cation radius which parallels that seen experimentally. In the liquid, the predicted total diffraction structure factors agreed well with the experimental ones at the large and small cation extremes (La and Al) but the agreement was poorer for intermediate size cations (e.g. Y^{3+}). The worst case was $ScCl_3$, where there was very little resemblance between the calculated and observed structure factors. Further consideration (summary of [12]) of the reasons for these failures led to a re-evaluation of the short range potential between the Cl^- ions. Below, we describe the considerations behind new potentials and in the remainder of the paper present the results of comparisons of simulation with the observed structures for crystals and neutron diffraction structure factors for the liquids across the whole range of MCl_3 systems.

2. Construction of the potentials

The potentials used consist of Born–Mayer-like pair potentials to describe the short range repulsion, dispersion and charge–charge interactions,

$$u_{ij}(r_{ij}) = B_{ij}e^{-(a_{ij}r_{ij})} + \frac{Q_iQ_j}{r_{ij}} - \frac{C_6^{ij}}{r_{ij}^6} - \frac{C_8^{ij}}{r_{ij}^8}. \quad (1)$$

These are supplemented by an account of polarization effects via the polarizable ion model introduced previously [23, 24]. Throughout, formal charges (Q_i) of +3 for cations and −1 for anions are used. The terms in C_6^{ij} and C_8^{ij} describe dispersion effects which, in practice, make little difference to calculated structures but do affect energetics.

In the first stages of this work, the parameters in the short range potential were determined from the Busing representation.

$$B_{ij} = f(\rho_i + \rho_j)e^{a_{ij}(\sigma_i+\sigma_j)} \quad (2)$$

and

$$a_{ij} = \frac{1}{\rho_i + \rho_j}, \quad (3)$$

where f is a constant, so that the properties of the pair interactions are derived from properties of the individual ions. σ_i is an ionic radius and ρ_i reflects the shape of its electron density, as perceived through the range of repulsive interactions. The Cl^- radius (and other properties, including the polarizability) were presumed to be the same in all the melts, so that the Born–Mayer potential between Cl^- ions was the same in all systems. In practice, the Coulomb repulsion between cations is so strong that the short range repulsion between cations is always negligible, as is the cation–cation dispersion, on account of the relatively small polarizability. The pair potentials were based upon potentials devised by Erbölükbas *et al.* (hereafter referred to as the EAT potential) and later used by Talipinar *et al.* [22], to fit Raman frequencies for a range of MCl_6^{3-} ions, to which minor modifications were made to the assumed radii of certain cations. The anion polarization [23] is controlled by two parameters: the Cl^- polarizability α, and the 'induction-damping' parameter b [23, 24]. The latter is the reciprocal of the length scale on which the dipole induced in an anion by a neighbouring cation deviates from the simple electric field-induced dipole due to short range effects. Therefore we scale b in accord with the sum of cation and anion radii (table 1),

$$b = c/(\sigma_+ + \sigma_-), \quad (4)$$

where the constant of proportionality $c = 7.42$, is the same as that used in MCl_2 systems. The polarizability of Cl^- was maintained at 20 au, the value appropriate to crystalline NaCl [25], possibly an underestimate for the systems of interest here.

This, then, was the 'generic' ionic potential referred to in section 1. It contains the implicit assumption that the Cl^- ion is the same entity in all the materials of interest and all phases, so that the only differences between different systems arise from the change in the cation radius. Unfortunately, it does not seem possible to account accurately for all the material properties with such a potential. In particular, in comparing the liquid structures with the neutron data we became aware [12] that although the cation–anion pair distribution function

Table 1. Potential parameters for the MCl_3 systems.

Ion pair	σ/Å	a_{ij}/au	B_{ij}/au	C_6^{ij}/au	C_8^{ij}/au	b/au
$Cl–Cl^{I}$	1.70	1.260	35.437	200.0	5000.0	—
$Cl–Cl^{II}$	—	1.670	128.249	200.0	5000.0	—
$Cl–Cl^{III}$	—	1.530	100.000	200.0	5000.0	—
La–Cl	1.42	2.439	10075.457	102.220	0.0	1.258
Ce–Cl	1.40	2.439	9188.352	102.220	0.0	1.267
Tb–Cl	1.30	2.439	5795.647	102.220	0.0	1.309
Dy–Cl	1.22	2.439	4008.61	0.0	0.0	1.340
Y–Cl	1.20	2.439	3655.663	45.815	0.0	1.354
Sc–Cl	1.12	2.250	1011.98	26.609	0.0	1.390
Fe–Cl	0.97	2.250	534.520	0.0	0.0	1.470
Al–Cl	0.90	2.250	396.785	0.0	0.0	1.512

(pdf) seemed to be predicted well by the model, the first peak in the Cl–Cl pdf was displaced to large r by ~0.1–0.2 Å. For this reason we have re-examined the representation of the Cl–Cl interactions in this work, leaving other aspects of the interaction model unchanged.

As we have stressed previously, the electron density around an anion in the condensed phase is strongly affected by its coordination environment, and this thereby changes its effective interactions with other ions. The effect has been studied with electronic structure calculations [26]. It is striking for the oxide ion, where different pair potentials must be used to describe the cation–anion interactions in (say) MgO in its 4-, 6- and 8-coordinate phases (zinc blende, rocksalt and CsCl) [27, 28]. With a single pair potential, errors in the relative energies of the different phases of order 100 kJ mol^{-1} arise. Alternatively, a single potential may be used, but one in which the effective ion radius (like σ above) is allowed to vary and adopt optimum values in a given coordination environment (a 'compressible ion' [27], or 'breathing shell' [29] model). For the Cl^- ion, electronic structure calculations have been performed for CsCl by Pyper [30], and he has shown that it is necessary to include the effect of ion compression in the potential in order to predict the correct ground state crystal structure (with a pair potential, the rocksalt structure emerges as more stable). However, the absolute energy errors associated with the pair potential are much smaller than for the oxide ion and, in general (except when two crystal phases are very close in energy, for example), it might be expected that pair potentials would work reasonably well for the Cl^- ion, thereby avoiding the technical complications of working with the compressible ion model [31]. However, it must be borne in mind that the pair potential reflects an average state of compression for the Cl^- ion *in the material of interest*, so that different potentials might be needed for different materials across the wide range of our study. In the way that our potential specification is based upon a Busing-like representation, this is not a problem for the cation–anion potential, where differences between the Cl^- ion can be taken up in the σ and ρ parameters. However, for the Cl–Cl potential we might expect that a single potential might not work equally well for all materials.

In order to get some non-empirical information on the Cl–Cl interactions we have fitted the Cl–Cl interaction energies which emerge from Pyper's *ab initio* study of CsCl to a pair potential. In figure 1 we contrast this pair potential (V^{II}_{ClCl}) for the short range repulsion with that used in our previous work [7, 12] (the 'EAT potential') and also the standard Fumi–Tosi (F-T) potential (as tabulated in [32]) used in much work on alkali and alkaline earth halides [24]. It can be seen that the *ab initio* potential agrees well with the F-T potential and is of shorter range than the EAT potential. This may reflect the greater degree of Cl^- ion compression

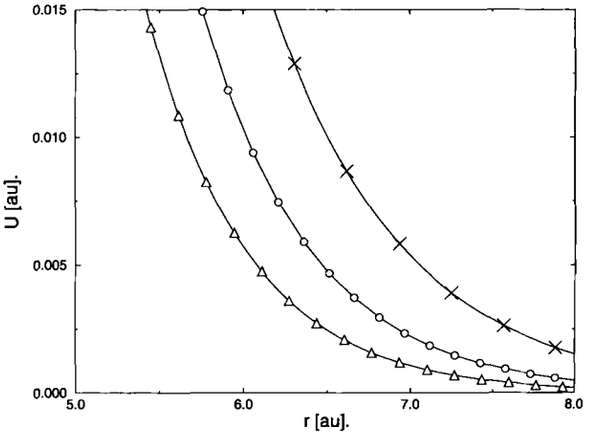

Figure 1. Comparison of Cl–Cl potentials considered: ×, EAT potential [21] (V^{I}_{ClCl}); △, *ab initio* potential for CsCl [30] (V^{II}_{ClCl}) which is very similar to the Fumi–Tosi potential; ○, intermediate potential (V^{III}_{ClCl}).

in the potentials determined for the alkali halides, where the anion coordination number is ~ 6, compared with the MCl_3 (EAT potential), where the coordination number is more likely to be 2 (MX_3 with an octahedrally coordinated cation). It should not be taken *a priori* to mean that the *ab initio* potential is to be preferred. For this reason, we have also examined another potential which is intermediate in range between the *ab initio* and EAT potentials. This is known as V^{III}_{ClCl} and is illustrated in figure 1.

One further point of interest which emerges from figure 1 is that the value of these potentials in the vicinity of the actual nearest Cl–Cl separations in the MCl_3 systems (7–8 au, 3.5–4 Å) is very small, and is dwarfed by the magnitude of the *pair* Coulomb potential at these distances. Therefore it is surprising to see the short range Cl–Cl potential playing such a strong role in refining our structural predictions.

All potential parameters are specified in table 1.

3. Crystal structures

The crystal structures adopted by the MCl_3 [12, 33, 34] systems provide an interesting insight into the interplay between the effects of ion size and polarization, and provide a stern test of the interaction potentials. The larger cations prefer higher coordination numbers and, because the cation–anion separation is larger, the polarization effects are smaller.

The YCl_3 structure is adopted by most of the intermediate and small cation systems (for cations smaller than Dy^{3+}, in table 1). The structure consists of planes of *edge*-sharing octahedra. Both the YCl_3 structure and the BiI_3 structure (adopted by $FeCl_3$) may be viewed as derived from a close-packed lattice of Cl^- ions with the cations in octahedral holes and differing only in the stacking sequence of the close-packed layers, the YCl_3 being cubic and BiI_3 hexagonal. As such, their energies are very similar. A picture of the YCl_3 structure appears on the cover of [34], from which it can be seen that the pattern of occupation of octahedral holes gives alternating planes of vacancies and two-thirds of the octahedral sites filled, thus creating a layered crystal structure in which the cations are crowded into a single layer and in which each plane of anions is sandwiched between a cation layer on one side and an anion layer on the other. Clearly the situation is unfavourable for the inter-ion Coulomb interactions but, as discussed previously in work on MX_2 systems [24, 35], the layered structure promotes a large negative polarization contribution to the lattice energy.

For the larger lanthanide ions, the octahedral holes in a close-packed anion lattice are too small to accommodate the cations, and so high coordination number structures are adopted, such as the UCl_3 and $PuBr_3$ structures. The UCl_3 structure is adopted by the largest cations and has a coordination number of anions about cations of 9, with the local symmetry around a cation a tricapped trigonal prism. This is the only 3-dimensional (i.e. non-layered) lattice formed by the trivalent metal chlorides. The $PuBr_3$ structure is adopted by cations of intermediate radii, as in $TbCl_3$ and the low temperature form of $DyCl_3$. The coordination in this structure is $[8 + 1]$. This is a layered structure with 8 neighbours in the same layer and the 9th neighbour lying in the adjacent layer at a slightly larger distance. The $PuBr_3$ structure can be described as consisting of triangular prisms with Pu^{3+} ions at the centres and the Br^- ions at the vertices. These prisms share triangular faces to form parallel columns. The UCl_3 structure can be described in terms of similar triangular columns, but the two structures differ in the way the columns are packed together. In the UCl_3 type structure there are three neighbouring columns arranged so that each U^{3+} ion has three Cl^- neighbours adjacent to the lateral faces of the prism (giving a tricapped prism). In the $PuBr_3$ there are four neighbouring columns, but only two of them provide a close Br^- neighbour to the Pu^{3+} ion. A ninth neighbour is in the direction of the third lateral face, but it is further away than the others. The UCl_3 and $PuBr_3$ crystal structures are expected to be very close in energy and molar volume, due to the similar local arrangements of the ions.

One other structure is relevant to our considerations for the smallest cation (Al^{3+}), although it is not adopted by any of the MCl_3 systems in practice. This is the $AlBr_3$ structure, which may be viewed also as a close-packed anion lattice but in which the cations occupy the *tetrahedral* holes and therefore have coordination number 4 rather than 6 as in the YCl_3 structure. It would therefore be expected to become significant for a small cation: anion radius ratio. It may be visualized, alternatively, as a molecular solid of Al_2Br_6 units [8], in which the highly asymmetric anion sites are clear. Such Al_2Br_6 units are overall charge neutral and so are held together by dispersion forces alone. As is well known, the local structure in *liquid* $AlCl_3$ is regarded as being composed of these dimers. Hence the energy of the $AlBr_3$ structure for $AlCl_3$ must be very close to that of the experimentally observed YCl_3 structure.

3.1. *Energy versus volume curves*

From the considerations above, we would expect that as we reduce the cation radius in the interaction potentials the lower coordination number structures ($AlBr_3$ < YCl_3 < $PuBr_3$ < UCl_3) should become progressively more stable. The challenge is to ensure that the change in the most stable structure occurs at the appropriate element. Thus we focus on the largest and smallest

cation systems (La and Al) and on two intermediate size systems (Tb and Y) with radii close to where the transition between the high coordination (UCl_3 and $PuBr_3$) and six-coordinate structure (YCl_3) occurs. Since our potentials depend only on the cation radius, the predictions for all cations in between these points should follow.

The structures are set up using idealized atomic positions in the unit cell (see [33, 34] and references therein), and then rescaled to a number of different total cell volumes without allowing any change in the *shape* of the unit cell. Structural relaxation of the ion positions within the cell was allowed. All the calculations were performed with Cl–Cl potential II, and the other potentials were as detailed in table 1. The number of ions used in the crystal calculations were as follows: UCl_3, 1120; $PuBr_3$, 768; YCl_3, 960; and $AlBr_3$, 960.

Figure 2 shows the internal energy *versus* cell volume for the relevant crystal structures for $AlCl_3$, YCl_3, $TbCl_3$, and $LaCl_3$ (parts (*a*)–(*d*), respectively), i.e. in order of increasing cation size. The results for two potentials for each material are shown: these involve the same cation–anion potential but, for the reasons we discussed above, we contrast the relatively long range anion–anion EAT potential (V^{I}_{ClCl}), used in our earlier work [12], to the short range *ab initio* potential (V^{II}_{ClCl}). The intermediate potential V^{III}_{ClCl} gives results between these extremes. The results with the new potential are shown by the darker lines, whereas the V^{I}_{ClCl} results are the lighter lines. The (approximate) common tangent to the lowest energy structures for a given potential are illustrated, with straight lines in the same shade. The gradient of the common tangent gives the (negative of) the pressure of a predicted phase tran-

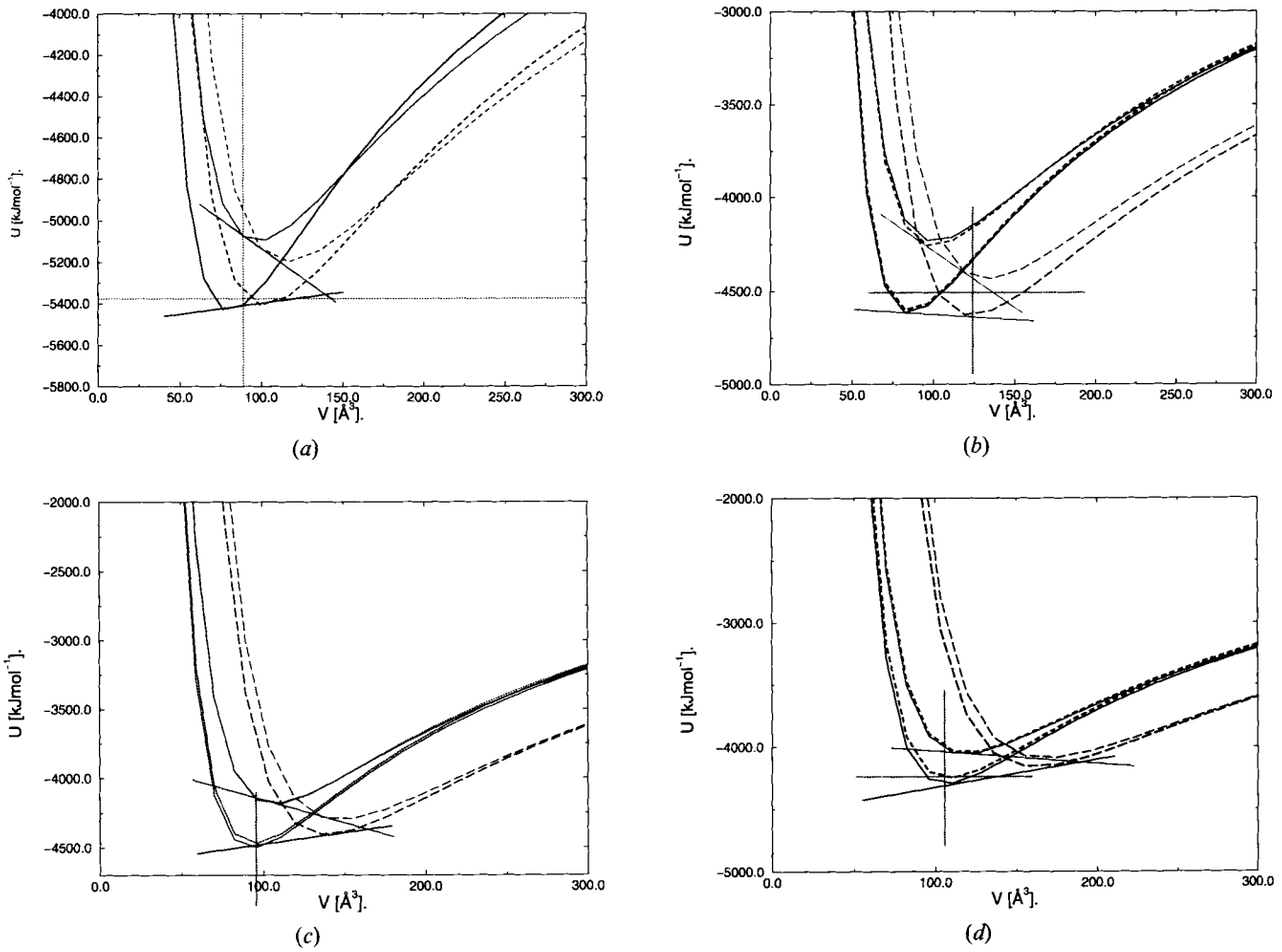

Figure 2. Energy–volume curves for the systems (*a*) $AlCl_3$, (*b*) YCl_3, (*c*) $TbCl_3$ and (*d*) $LaCl_3$: (*a*) solid line, YCl_3 structure and dashed line, $AlBr_3$ structure; (*b–d*) solid line, UCl_3 structure, short dashed line, $PuBr_3$ and long dashed line, YCl_3. In all cases the lighter (upper) lines are calculated used the EAT (V^{I}_{ClCl}) potential and the darker lines with the *ab initio* potential (V^{II}_{ClCl}). The horizontal and vertical lines highlight the location of the experimental lattice energy and volume where available.

sition between the two structures. The experimental lattice energies (deduced in the main from Born–Haber analyses of the data to be found in [36]) and molar volumes of the crystals are indicated by the dashed lines.

3.1.1. *$LaCl_3$*

We focus first on largest cation (La) in figure 2(*d*). Here we see that the high coordination number structures (UCl_3 and $PuBr_3$) are predicted to be considerably lower in energy compared with the YCl_3, provided that the V^{II}_{ClCl} (*ab initio*) potential is used. With the potential used in the previous work, these structures are predicted to be unstable with respect to the YCl_3. Furthermore, with V^{II}_{ClCl}, the UCl_3 structure is predicted to be the most stable, with a cell volume and lattice energy in good agreement with experiment. Scanning all the results (figure 2(*a–d*)) we see the progressive stabilization of the higher coordinate structures with increasing cation size. For $LaCl_3$, the $AlBr_3$ structure is at such high energy that it has been omitted from the figure. As we remarked earlier, in view of the small value of this potential compared to the pair Coulomb potential at the range of Cl–Cl distances of interest, it is surprising to see it play such an important role in the crystal structures.

3.1.2. *$AlCl_3$*

For the smallest cation (Al) system (figure 2(*a*)), both the high coordination number (UCl_3 and $PuBr_3$) structures are of very high energy compared with the YCl_3 and $AlBr_3$ structures and are omitted for clarity. We see that the minima of the latter two structures are of very similar energies, with the minimum energy of the $AlBr_3$ structure at a higher molar volume than the YCl_3. That these structures should have such similar energies and different volumes is in accord with the fact that the coordination number of the aluminium does change from 6 to 4 across the melting transition in $AlCl_3$, and that this results in an anomalously large increase in the molar volume. Upon close inspection we see that only for the *ab initio* potential V^{II}_{ClCl} is the YCl_3 structure predicted to be stable with respect to the $AlBr_3$. The minimum of the YCl_3 U/V curve indicates the lattice energy and molar volume are both slightly lower than the experimental value, and also indicates that, in order to get an optimal representation of the observed *crystal* structure, some further optimization of the cation–anion potential is required.

Thus we see that at both ends of the cation size range, the V^{II}_{ClCl} potential seems to predict the order of structure energies much better than the other potentials used. These tend to over-stabilize the less tightly bound, low coordination number structures as a consequence of the large effective size of the Cl^- ions in the short range Cl–Cl interaction. This inhibits the dense packing of the chloride ions in the UCl_3 structure in $LaCl_3$ and in the YCl_3 in $AlCl_3$ at the experimental densities.

3.1.3. *$TbCl_3$ and YCl_3*

$TbCl_3$ and YCl_3 bridge the range of ionic radii in which the transition between the high and 6-coordination numbers occurs. The predicted U/V curves are shown in figure 2(*c*, *b*). It can be seen that, with V^{II}_{ClCl}, the minimum energies for the UCl_3 and $PuBr_3$ structures are indeed very similar to that of the YCl_3. For the other potentials, the YCl_3 structure is considerably more stable, even in $TbCl_3$, in disagreement with experiment.

For $TbCl_3$, the UCl_3 structure is predicted to be slightly more stable than the $PuBr_3$ with V^{II}_{ClCl}. In reality the $PuBr_3$ is believed to be of lower energy. Gunsilius *et al.* [37] observed that a metastable UCl_3 structured material could be prepared and that at 700 K it underwent an irreversible transition to the $PuBr_3$ structure, which indicates just how close their energies are. The balance between the two structures is very subtle, since the local coordination arrangements within them are very similar. It can be seen that even by changing to V^{I}_{ClCl} the predicted order of stability is reversed. No lattice energy is available for $TbCl_3$, but the observed molar volume is very close to the position of the minimum in the $PuBr_3$ (and UCl_3) U/V curves.

For YCl_3 the experimentally observed crystal structure is found to be most stable with V^{II}_{ClCl}. The molar volume is in very good agreement with experiment but the lattice energy appears to be a little high. The calculations indicate that there should be a phase transition to the high coordinate structures at very low applied pressure. However, because the transition would involve a major reorganization of the local coordination arrangement, it is likely that a very large barrier to this transition exists, which might preclude its observation.

3.1.4. *Summary*

Using the anion–cation pair potentials introduced previously, and a new, shorter range anion–anion repulsive potential (V^{II}_{ClCl}), the predicted crystal structures are brought into good agreement with experimental observation across the range of materials of interest.

4. The liquid phase

For the liquid phase simulations each MD run was performed at or near the temperature at which diffraction experiments were undertaken and at the deduced experimental density, as quoted in [13–18] (see table 2). These densities have not always been directly measured and could be a source of significant uncertainty. Except where noted below, simulations were carried out with

Table 2. Temperatures and densities used in the simulations of the MCl_3 liquids along with the simulated and experimental cation–anion coordination numbers.

System	Temperature/K	Density/g cm^{-3}	CN (sim.)	CN (exp)
$LaCl_3$	1178	3.174	7.9	8.2
$CeCl_3$	1108	3.234	—	—
$TbCl_3$	900	3.580	7.2	7.5
YCl_3	1033	2.492	6.6	6.2
$ScCl_3$	1253	1.643	5.6	5.2
$AlCl_3$	600	1.277	4.0	4.0

500 ions. Simulations were carried out for the full range of materials on which experiments have been undertaken and using the three Cl–Cl potentials described above. In the interests of brevity, we will present only results for the systems $LaCl_3$, $TbCl_3$, YCl_3, $ScCl_3$ and $AlCl_3$ below, and we will normally give results only for the potential which gave the best agreement with the experimental diffraction data. For $LaCl_3$, $TbCl_3$, YCl_3 and $AlCl_3$ the results may be compared with those published previously [7, 12], which were obtained with the V^{I}_{ClCl} (EAT) potential; in all these cases, substantial improvements in the (already respectable) agreement with experiment are found. For $ScCl_3$ simulation results are presented for the first time: with the old potential we were unable to obtain any resemblance to the observed diffraction pattern. The crystal structures of all the materials except $ScCl_3$ have been discussed above, as they were on the boundaries between different structure types. Sc^{3+} is intermediate in cation size between Y^{3+} and Al^{3+} and is comfortably in the stability range of the YCl_3 structure, which is predicted as the most stable with all three potentials.

4.1. *Comparison of simulated and experimental structures*

Partial (Ashcroft–Langreth) structure factors $S_{\alpha\beta}(k)$, can be calculated both by directly averaging over the correlation functions of the Fourier components of the ion densities,

$$S_{\alpha\beta}(k) = (N_\alpha N_\beta)^{-1/2}\left\langle \sum_{i\in\alpha}\sum_{j\in\beta} \exp\left[i\mathbf{k}\cdot\mathbf{r}_{ij}\right]\right\rangle, \quad (5)$$

and also by Fourier transformation of the partial pair distribution functions $g_{\alpha\beta}$,

$$S_{\alpha\beta}(k) = \delta_{\alpha\beta} + 4\pi n_0 (c_\alpha c_\beta)^{1/2}\int \mathrm{d}r (g_{\alpha\beta}(r) - 1) r \frac{\sin(kr)}{k}, \quad (6)$$

where c_α is the mole fraction of species α and n_0 is the ionic number density. At low k, the former method (when using $\mathbf{k}$ vectors commensurate with the simulation cell) gives a more reliable structure factor, since it is free of truncation errors. The functions displayed in the current work are obtained by combining the direct averages, for $k \leqslant 2\,\text{Å}^{-1}$, with the Fourier transformed pdfs for larger k values.

The total (neutron weighted) structure factor, for comparison with experiment, is given by

$$F(k) = b_M^2 c_M [S_{MM}(k) - 1] + 2 b_{Cl} b_M (c_{Cl} c_M)^{1/2} S_{MCl}(k) + b_{Cl}^2 c_{Cl} [S_{ClCl}(k) - 1], \quad (7)$$

where b_α is the coherent neutron scattering length of species α. Neutron scattering lengths are taken from [38].

By Fourier transformation of the experimental structure factor $F(k)$, the neutron-weighted radial distribution function may be obtained:

$$G(r) = \frac{1}{2\pi^2 n_0}\int_0^\infty \mathrm{d}k\, k \frac{\sin(kr)}{k} F(k) = b_M^2 c_M^2 (g_{MM} - 1) + 2 b_{Cl} b_M c_{Cl} c_M (g_{MCl} - 1) + b_{Cl}^2 c_{Cl}^2 (g_{ClCl} - 1). \quad (8)$$

4.1.1. *$AlCl_3$*

As with the crystals, we begin with the extreme large and small cation ($LaCl_3$ and $AlCl_3$) systems for which, for different reasons, the experimental information is particularly sensitive to the Cl–Cl structures. For $AlCl_3$ the calculated total neutron scattering structure factor obtained with the intermediate potential V^{III}_{ClCl} is compared with the experimental data of Badyal *et al.* [8] in the upper panel of figure 3. In the lower panel, the neutron-weighted partials are shown. These indicate that the shape of the total neutron structure factor is dominated by S_{ClCl}. Note that we have used a different Cl–Cl interaction potential for the liquid from the potential that predicts the correct order of crystal energies: one which corresponds to a slightly larger Cl^- ion.

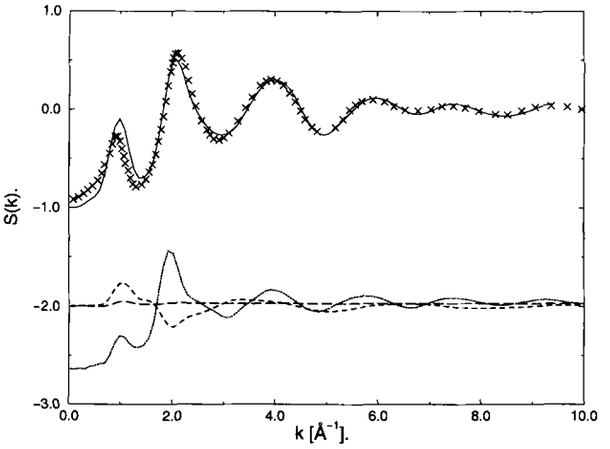

Figure 3. Simulated total neutron weighted structure factor (solid line) for $AlCl_3$ compared with the experimental total structure factor (×). The neutron-weighted partial structure factors defined in equation (7) are shown below shifted by a constant of −2. Dotted line, $S_{ClCl}(k)$; dashed line, $S_{AlCl}(k)$; and long dashed line, $S_{AlAl}(k)$.

V^{III}_{ClCl} is found to give a better liquid structure factor for $AlCl_3$ than the 'best' crystal potential V^{II}_{ClCl} and also slightly better than that obtained with the EAT potential in our original work [7]. Snapshots of the simulation cell indicate that the liquid is composed largely of Al_2Cl_6 dimers. As these are of very similar appearance to the snapshot appearing in our original work [7], they are not repeated here. With the crystal potential V^{I}_{ClCl}, there is some tendency for these dimers to associate, so that larger clusters containing short chains of 4-coordinate Al^{3+} ions which share a single Cl^- ion are evident. Such molecules are not thought to feature in liquid $AlCl_3$, though their presence is inferred (from the higher conductivity) in the slightly larger cation system $FeCl_3$ [39]. These considerations suggest that in the best description of $AlCl_3$ we need a slightly larger Cl^- ion in the liquid than in the crystalline phase. A physical reason for this could be that, because of the substantial volume increase on melting, the Cl^- ion is allowed to relax from its compressed state in the crystal.

4.1.2. *$LaCl_3$*

Figure 4(*a*) shows a comparison between the total neutron structure factor for $LaCl_3$ and the results predicted with potentials V^{III}_{ClCl} and V^{I}_{ClCl}, as used in our previous work. From the lower panel, showing the partials, it can be seen that in this case the total structure factor contains significant contributions from both S_{ClCl} and S_{LaCl} for all k. A significant improvement is noted with the new potential, and the structure factor calculated with this potential is significantly better than that obtained with the best crystal potential, as was the case for $AlCl_3$. The origin for the improvement can be seen by comparing the structure in real space. Figure 4(*b*) compares the experimental neutron-weighted pdf with that calculated from the simulations with potentials V^{III}_{ClCl} and V^{I}_{ClCl}. In the lower panel, the partial pdfs calculated with V^{III}_{ClCl} are shown, which make clear the origin of the features appearing in the total. The major difference between the two simulations occurs in the position of the second peak in the pdf which, as is clear from the partials, corresponds to the first peak of the Cl–Cl pdf. The smaller size of the Cl^- ions in the new potentials allows a closer approach of the Cl^- ions. For the crystal potential, an even closer approach would be allowed.

Good approximations to the partial structure factors can be obtained from the experimental data by taking difference functions of the total structure factors for systems with very similar physiochemical properties. Salmon and Wasse [14] have applied this principle to their data for $LaCl_3$ and $CeCl_3$, noting that the ionic radii of La and Ce are very similar. This assumes that $LaCl_3$ and $CeCl_3$ are structurally the same (isomorphic) and differ only in the neutron scattering lengths of the cations. Assuming $S_{LaLa}(k) = S_{CeCe}(k) = S_{MM}(k)$ and $S_{LaCl}(k) = S_{CeCl}(k) = S_{MCl}(k)$ then the first-order difference function $\Delta_M(k)$ is given by

$$\Delta_M(k) = S_{LaCl_3}(k) - S_{CeCl_3}(k). \tag{9}$$

This function is dominated by the cation–anion correlations and is found to be very insensitive to the differences between our different Cl–Cl potentials. On the other hand, the cation–anion correlations can be removed by forming the difference function $\Delta F'(k)$ defined as

$$\begin{aligned}\Delta F'(k) &= S_{LaCl_3}(k) - [b_{La}/(b_{La} - b_{Ce})]\Delta_M(k) \\ &= K^*_{ClCl}[S_{ClCl}(k) - 1] - K^*_{MM}[S_{MM}(k) - 1],\end{aligned} \tag{10}$$

where

$$\left.\begin{aligned} K^*_{MM} &= b_{La}b_{Ce}c_M, \\ K^*_{ClCl} &= b^2_{Cl}c_{Cl}. \end{aligned}\right\} \tag{11}$$

Using tabulated scattering lengths for LA^{3+}, Ce^{3+} and Cl^- [38], it is found that $K^*_{MM} = 99.6$ mbarn and $K^*_{ClCl} = 688$ mbarn, i.e. the anion–anion correlations account for 87% of $\Delta F'(k)$. Therefore this should provide a good way of examining the Cl–Cl correlations in the liquid.

The $\Delta F'(k)$ calculated with the new potential are shown in figure 4(*c*) and compared with values obtained with the EAT Cl–Cl potential (V^{I}_{ClCl}). The agreement between experiment and calculation is much better with the new potential (V^{III}_{ClCl}). In particular, the amplitude of the first two peaks is much improved and the

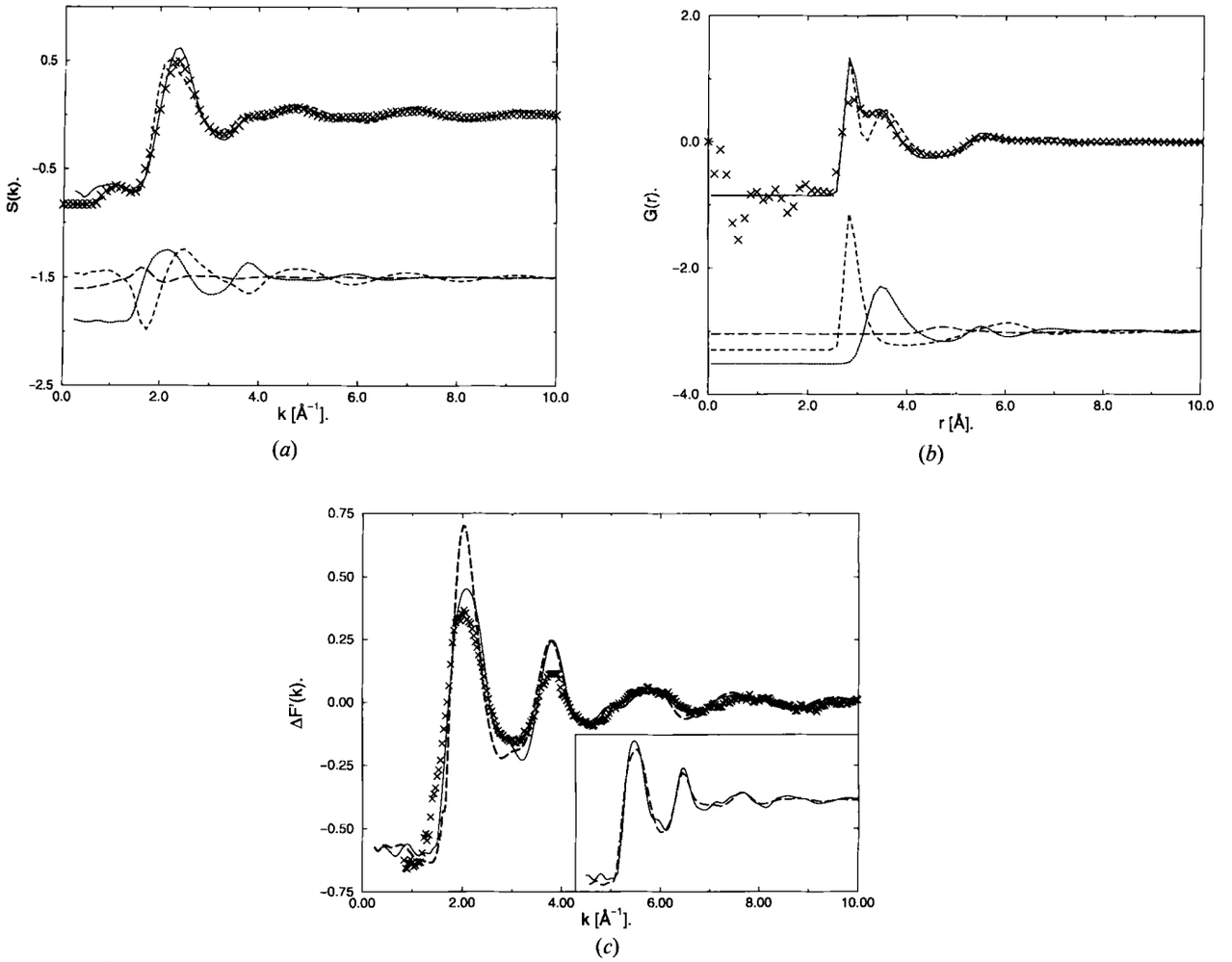

Figure 4. (*a*) Simulated total neutron weighted structure factor (solid line) for $LaCl_3$ compared with the experimental total structure factor (×), with the neutron-weighted partials shown below shifted by a constant of −1.5. Lines as for figure 3. The dashed line shows the simulated total function using the EAT potential (V^{I}_{ClCl}) from [12]. (*b*) The corresponding real-space data with the neutron-weighted partial pdfs shifted by a constant of −3. Lines as for (*a*). (*c*) The difference function $\Delta F'(k)$ obtained by using the isomorphous assumption from the data for $LaCl_3$ and $CeCl_3$: ×, experimental data [14]; solid line, simulated difference using V^{III}_{ClCl}; and dashed line, simulated difference using V^{I}_{ClCl}. The inset shows the similarity between the simulated difference function with V^{III}_{ClCl} and the pure Cl–Cl partial structure factor (dashed line) calculated with the same potential.

experimental and calculated data are now in phase for large values of k. Also indicated in the inset to figure 4(*c*) is the close correspondence between $\Delta F'(k)$ and the single $S_{ClCl}(k)$ partial.

4.1.3. *$TbCl_3$*

In figure 5(*a*) the experimental and simulated total neutron weighted structure factors for the melt are compared along with the simulated neutron weighted partial structure factors. The simulation data are obtained with V^{III}_{ClCl}. The quality of agreement is excellent, similar to that reported above for $LaCl_3$, and better than the agreement reported in [12] for $TbCl_3$ with the old potential. The position of the pre-peak (at ~ 1 Å^{-1}) is good; note that it has shifted to lower k compared with $LaCl_3$ and become more prominent. At first sight this is somewhat surprising, as a shift to lower k means that the corresponding real space feature has moved to larger r, whereas the size of the cation has become smaller on passing from La to Tb. We will discuss below how the reduction of cation size increases the length scale of the intermediate range order.

The total and partial pdfs for $TbCl_3$ are shown in figure 5(*b*). We have previously noted an excessive 'sharpness' of peaks in the total $G(r)$ compared with those generated from experiment; a good example is

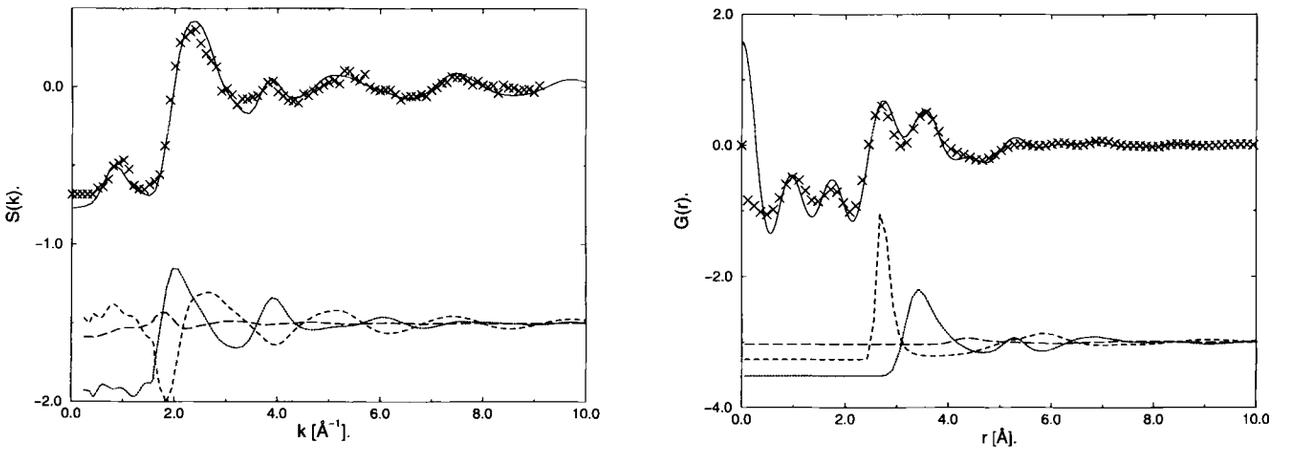

(*a*) (*b*)

Figure 5. As for figure 4 but for $TbCl_3$. The partial structure factors have been shifted by a constant of -1.5 in (*a*) and -3 in (*b*).

seen in the $LaCl_3$ data above (figure 4(*b*)). In the experiments the diffraction data are gathered over a restricted range of scattering angles, so that the real space distribution function is subject to truncation errors. In the case of the $TbCl_3$ data the data were gathered only to $10\,Å^{-1}$. In figure 5(*b*) we have calculated the total pdf (upper panel) by back-transforming the *simulated* total structure factor, applying a cutoff in the transform in order to replicate the experimental procedure. The cut off is chosen so that the low r oscillations match those in the experimental data in period and phase, which occurs with a cutoff at $8\,Å^{-1}$. It can be seen that these simulation results are much closer to the experimental data in the width and height of the first peak than the straight partial pdfs shown in the lower part of the figure. This suggests that at least part of the discrepancy between the heights and widths of the first peaks is due to truncation of the back-transform. However, it does not appear to be the whole story. For $TbCl_3$ the cutoff value of k is particularly small: applying the same procedure as above to the other systems' data produces a much smaller degree of broadening and leaves the first peak in the simulation $G_{tot}(r)$ still significantly narrower than the experimental function. A full resolution of these discrepancies should involve comparisons with other experiments which are particularly sensitive to the first-shell structure, notably EXAFS and X-ray diffraction, and is the subject of ongoing work.

4.1.4. *$ScCl_3$*

Comparison of simulated and experimental [15] structure factors and pdfs for $ScCl_3$ are shown in figure 6(*a*, *b*). The Sc^{3+} cation is intermediate in size between Y^{3+} and Al^{3+}. The structure factor shows a number of remarkable features, which we were completely unable to replicate in the earlier work. The most striking of these is the very prominent pre-peak (or 'first sharp diffraction peak') in the structure factor at $0.7\,Å^{-1}$. This is the signature of intermediate range order in the melt associated with a characteristic length scale of $\sim 10\,Å$. Also, the principal peak (which would be expected at about $2\,Å^{-1}$ ($\sim(2\pi/(\sigma_+ + \sigma_-))$) has disappeared and been replaced with a very broad feature extending over about $2\,Å^{-1}$. The simulation structure factors were obtained with the V^{III}_{ClCl} Cl–Cl potential, as for the other liquid systems discussed so far, and good agreement is seen between the calculated and experimental totals.

The length scale associated with the pre-peak is so large as to suggest that the periodic boundary conditions might affect the simulated structure. We therefore undertook additional calculations on a very large cell containing 6880 ions, in which the periodic repeat distance is more than doubled. The total structure factors calculated in the small and large cells are both shown in the figure. They are very similar, and the only noticeable difference lies in the position and height of the pre-peak, which moves to slightly lower k and broadens in the larger cell, bringing its appearance into better agreement with experiment. We will describe the real-space structures responsible for the pre-peak in the next section.

The partial structure factors shown in the lower panel make clear the reason for the 'disappearance' of the principal peak. The principal peaks of the Sc–Sc and Cl–Cl partials are very close together at about $2\,Å^{-1}$ (indicating that the nearest-neighbour cation–cation and anion–anion separations are very similar, which is not what would be expected given the triply-charged nature of the cations) and these are cancelled by the negative peak in the cation–anion partial. The

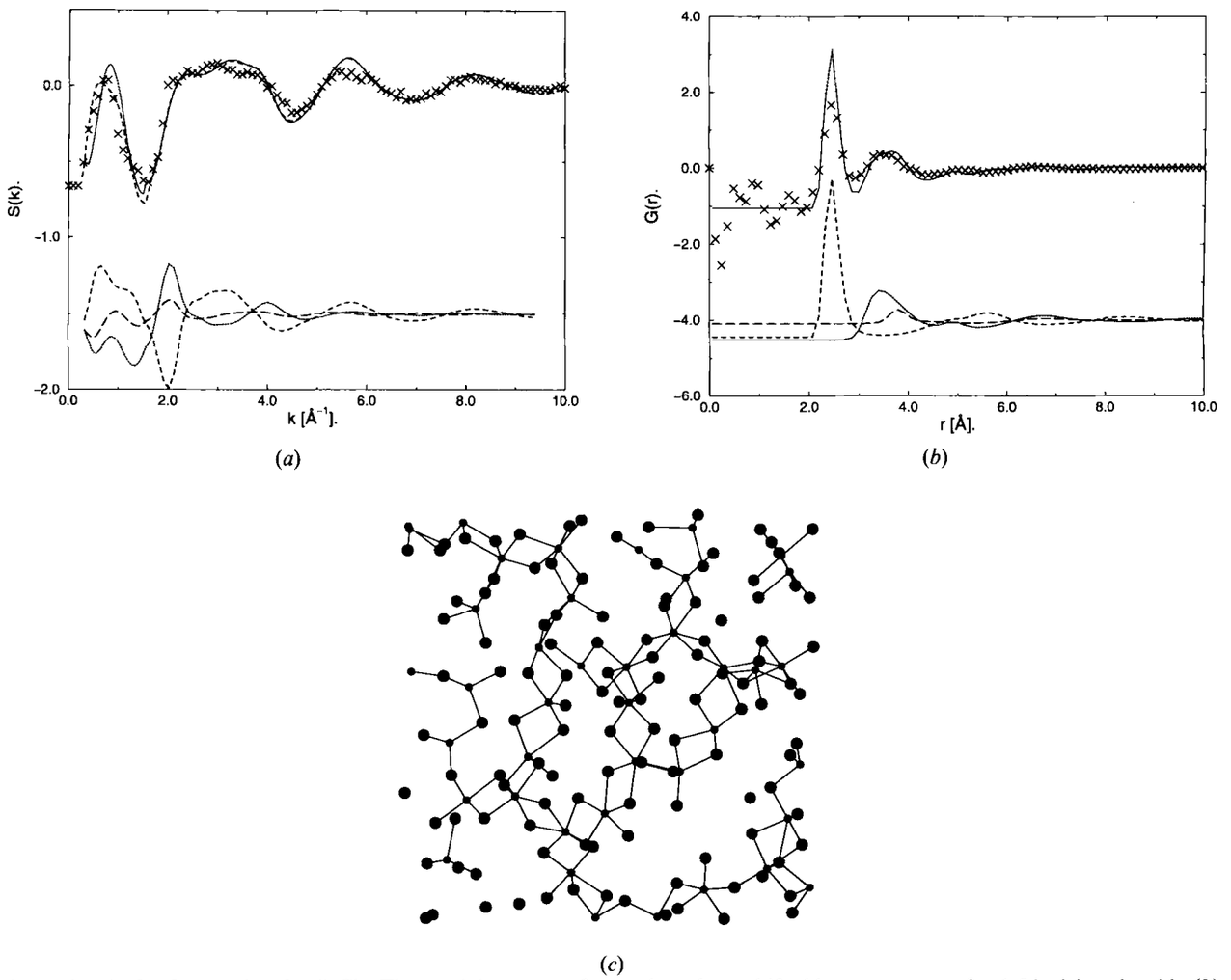

(*a*) (*b*) (*c*)

Figure 6. As for figure 4 but for $ScCl_3$. The partial structure factors have been shifted by a constant of -1.5 in (*a*) and -4 in (*b*). The upper dashed line in (*a*) is the total structure factor from a larger system of 6880 ions. (*c*) A molecular graphics snapshot of the liquid $ScCl_3$ showing the edge-linked chain structural motif. The large circles represent the Cl^- anions and the smaller circles the Sc^{3+} cations.

remaining broad feature reflects, predominantly, the shape of the cation–anion partial in this region. The similarity of the nearest-neighbour cation–cation and anion–anion separations is confirmed in the pdfs, shown in figure 6(*b*). As we have seen elsewhere [40, 41], and will discuss further below, this drawing together of the (highly charged) cations is attributable to the polarization effects, which induce a significant degree of edge-sharing between the coordination polyhedra around each ion.

4.1.5. *YCl_3*

Y^{3+} is similar in size to Dy^{3+}, Ho^{3+} and Er^{3+}. $HoCl_3$ and $ErCl_3$ were studied alongside YCl_3 in Wasse and Salmon's work [16, 18], and shown to exhibit similar structural features. YCl_3 had earlier been studied by Saboungi *et al.* [42], the two experimental total structure factors agreeing well. They show a significant pre-peak, though not as large as that appearing in $ScCl_3$, and not at such a low value of k. Furthermore, like $ScCl_3$, in place of a principal peak there is a broad maximum, extending over the range $\sim$2–4 Å^{-1}. In our previous work, using the V^{I}_{ClCl} Cl–Cl potential, we found it difficult to reproduce this feature. The total structure factor calculated with the old potential is shown by the dashed line in figure 7(*a*), to emphasize the discrepancies. In the present work, we have also been unable to reproduce the feature using the V^{III}_{ClCl} potential, which has been used for all the liquid simulations discussed so far. In fact, for YCl_3, and for the similarly sized $DyCl_3$ [19], we have obtained the best results with the same Cl–Cl potential as used for the crystals, i.e. the short-range potential

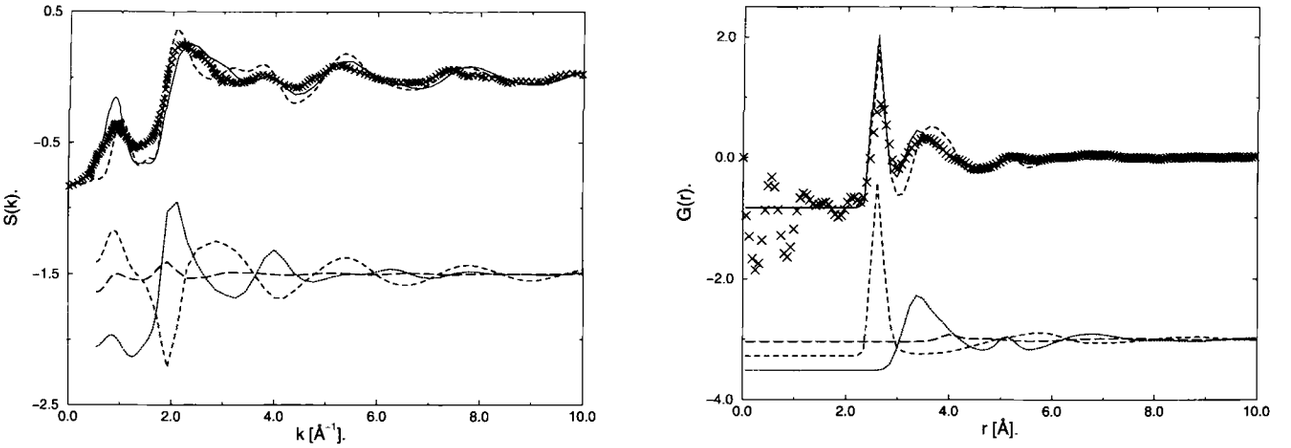

(*a*) (*b*)

Figure 7. As for figure 4 but for YCl_3. The partial structure factors have been shifted by a constant of -1.5 in (*a*) and -3 in (*b*). The upper dashed line in both (*a*) and (*b*) is the total structure factor calculated using the EAT potential (V^{I}_{ClCl}) from [12].

V^{II}_{ClCl}. The results obtained with this potential are shown by the full line in the figure. As can be seen from the partials, shown in the lower panel, the broad feature arises from interference between the cation–anion and anion–anion partials. In real space (figure 7(*b*)) we see that changing the Cl–Cl potential has brought the first peak in the Cl–Cl pdf to considerably smaller r, and into better accord with the position of the second peak in the neutron-weighted pdf. Were the structure factors for YCl_3 and $DyCl_3$ to have been calculated with the 'normal' Cl–Cl potential (V^{II}_{ClCl}), used for the other liquid systems, the quality of this comparison would have been much poorer (similar to that shown in the calculations done with the old potential). A less *ad hoc* justification for making an exception of Y and Dy, and using the same potential for the crystal and liquid, is the very close similarity of the liquid and solid densities for these materials. It could be argued that for these materials, which experience a volume change on melting of order only 1%, the Cl^- electron density does not relax on melting in the same way as occurs for the systems where, typically, the molar volume increases by ~20%, or more for $LaCl_3$, $TbCl_3$, $ScCl_3$ and $AlCl_3$.

4.2. *Discussion of the liquid structures*

Table 2 presents values for the coordination numbers of anions around cations for each of the simulations with the optimum potentials. The values are obtained by integrating the cation–anion pdfs to the position of the first minimum. The values are compared with the results from the neutron studies. Surprisingly good agreement is found, considering the different shape of first peaks of our pdfs and of the neutron data. Furthermore, in the neutron data, the first peak (due to M–Cl correlations) and the second (due to Cl–Cl correlations) of the neutron radial distribution function overlap rather strongly, but our analysis (based simply on the simulated MCl partial) supports the neutron values.

The results for the coordination numbers of the larger cation systems, which show a coordination number of about 8, are controversial. Raman studies of these systems suggest octahedral coordination, even in the pure melt. Also, older X-ray studies [43] were interpreted in terms of octahedral coordination. A full resolution of this controversy will probably await the separation of partial pdfs using isotopic substitution methods. To date, such studies have been made only for the intermediate size cation Dy^{3+} [19], which all studies agree is basically octahedrally coordinated (Dy^{3+} is very similar to Y^{3+}, both experimentally and in our simulation models). Also there are ongoing efforts to reconcile results from neutron, X-ray and EXAFS studies with the computer simulations, which hopefully will lead to a consensus.

For intermediate size cations, ranging in size from about Y^{3+} (or Dy^{3+}) to Sc^{3+}, the chloride melts are predominantly octahedrally coordinated, with average coordination numbers slightly higher than for the larger members and lower for the smaller. These coordination polyhedra are linked together into a network, with a considerable degree of edge-sharing. A snapshot of the instantaneous structure of the $ScCl_3$ melt is shown in figure 6(*c*). Only a slice of the simulation cell is shown, so that there are a number of ions which are disconnected from their actual neighbours. Nevertheless, the picture shows five- and six-coordinate Sc^{3+} linked together with a very high degree of edge-sharing to form a cross-linked network. The structure supports a

number of voids, and it is these inter-void correlations which are responsible for the prominent, low-k pre-peak in the structure factor [44]. We have previously [12] presented snapshots of the other liquids studied here, which were simulated with the old potential. The change in Cl–Cl potential has had little effect on the qualitative picture which emerges from these snapshots, and so we have not repeated them here. We have also argued, in exploring the link between the structures of chloride and bromide melts [45], that the intermediate size cation systems form a different liquid structure class from the larger cation systems, which can be recognized from the different shape of the structure factor (replacement of the principal peak by a broad maximum; existence of a prominent pre-peak). The distinction appears to coincide with the transition, as the cation size is reduced from the high coordination (UCl_3 and $PuBr_3$) crystal structures to the YCl_3, in the solid phase. Except for the striking exception of $AlCl_3$ (and $FeCl_3$), our studies would support the general precept that the local order in the solid phase and that in liquid phase are closely related [1].

5. Conclusions

We have used the results obtained from recent neutron diffraction studies of the liquids [13–18] and the existing information on the crystal structures to refine a representation of the interactions across the range of MCl_3 systems. The potentials used are ionic ones, in the sense that they represent closed shell interactions between species carrying formal charges. The polarization effects play a key role in reproducing the structures in the liquid and solid phases. Nevertheless, in optimizing the simulations, we have had to depart from the ionic model ideal, as expressed in the Busing potential, that all potential parameters should be derived from properties of the individual ions, and that the same potentials should be used in all phases. The shortcomings of this approach appear to be related to the idea that the anion changes its effective size in different environments [26, 27] which, in the particular representation we have used in this work, has manifested itself in the need to use a different Cl–Cl short range repulsive potential in different phases. For the most part we have had, effectively, a larger Cl^- ion in the liquid rather than the crystal. The exceptions are for YCl_3 and $DyCl_3$, where the volume change on melting is very small, and the crystal potential performs best for both phases. In principle we should also allow for this change of anion size in the cation–anion potential, but this has not been proven necessary to obtain the results we have demonstrated. The fact that we have had to focus on the anion–anion interactions, when the conventional view of ionic systems is that the like ion interactions are dominated by the Coulomb repulsion, is probably due to the stoichiometry, which necessitates a relatively close approach of the anions in the condensed phase.

The potentials will enable detailed studies of other properties of these fascinating liquids (as exemplified by the intriguing microstructure seen in figure 6(c)). Foremost among the objectives is to reconcile the information on the local structure which emerges from the diffraction techniques, EXAFS and Raman. The transport properties are also of great interest, as well as the coordination chemistry when the pure materials are dissolved in structure-breaking melts.

The work was supported by EPSRC through the EPSRC Liquids Network, Grant GR/L/49369 and a studentship for F.H. Some of the calculations were done at the Oxford Supercomputer Centre. M.W. thanks the Royal Society for a Research Fellowship. We are grateful to Phil Salmon and Jonathan Wasse for numerous discussions about their experimental results.

References

[1] Rovere, M., and Tosi, M. P., 1986, *Reports Progr. Phys.*, **49,** 1001.
[2] Tosi, M. P., Price, D. L., and Saboungi, M.-L., 1993, *Ann. Rev. phys. Chem.*, **44,** 173.
[3] Enderby, J. E., and Barnes, A. C., 1990, *Reports Progr. Phys.*, **53,** 85.
[4] Wei, D., and Okido, M., 1997, *Current Topics Electrochem*, **5,** 21.
[5] Matsuura, H., Takagi, R., Zbalocka-Malicka, M., Rycerz, L., and Szczepaniak, W., 1997, *J. nucl. Sci. Technol.*, **33,** 895.
[6] Photiadis, G. M., Borrensen, B., Papatheodorou, G. N., 1998, *J. chem. Soc. Faraday. Trans*, **94,** 2605.
[7] Hutchinson, F., Walters, M. K., Rowley, A. J., and Madden, P. A., 1999, *J. chem. Phys.*, **110,** 5829.
[8] Badyal, Y. S., Allen, D. A., and Howe, R. A., 1994, *J. Phys. Condens. Matter*, **6,** 10193.
[9] Badyal, Y. S., Saboungi, M.-L., Price, D. L., Haeffner, D. R., and Shastri, S. D., 1997, *Europhys. Lett.*, **39**(1), 19.
[10] Harris, R. L., Wood, R. E., and Ritter, H. L., 1951, *J. Amer. chem. Soc.*, **73,** 3151.
[11] Akdeniz, Z., Caliskan, M., Cicek, Z., and Tosi, M. P., 2000, *Z. Naturf.* A, **55,** 575; Akdeniz, Z., and Tosi, M. P., 1992, *Proc. R. Soc. Lond.* A, **437,** 85.
[12] Hutchinson, F., Rowley, A. J., Walters, M. K., Wilson, M., Madden, P. A., Wasse, J. C., and Salmon, P. S., 1999, *J. chem. Phys.*, **111,** 1.
[13] Wasse, J. C., and Salmon, P. S., 1998, *Physica* B, **241–243,** 967.
[14] Wasse, J. C., and Salmon, P. S., 1999, *J. Phys. Condens. Matter*, **11,** 1381.
[15] Wasse, J. C., and Salmon, P. S., 1999, *J. Phys. Condens. Matter*, **11,** 2171.

[16] WASSE, J. C., and SALMON, P. S., 1999, *J. Phys. Condens. Matter*, **11,** 9293.
[17] WASSE, J. C., SALMON, P. S., and DELAPLANCE, R. G., 2000, *Physica*, **276,** 433.
[18] WASSE, J. C., 1998, Ph.D. thesis, University of East Anglia.
[19] TAKAGI, R., HUTCHINSON, F., MADDEN, P. A., ADYA, A. K., and GAUNE-ESCARD, M., 1999, *J. Phys. Condens. Matter*, **11,** 645.
[20] HUTCHINSON, F., 2000, D.Phil. thesis, University of Oxford.
[21] ERBÖLÜKBAS, A., AKDENIZ, Z., and TOSI, M. P., 1992, *Nuovo Cimento* D, **14,** 87.
[22] TATLIPINAR, H., AKDENIZ, Z., PASTORE, G., and TOSI, M. P., 1992, *J. Phys. Condens. Matter*, **4,** 8933.
[23] WILSON, M., MADDEN, P. A., and COSTA-CABRAL, B. J., 1996, *J. phys. Chem.*, **100,** 1227.
[24] MADDEN, P. A., and WILSON, M., 1996, *Chem. Soc. Rev.*, **25,** 339.
[25] FOWLER, P. W., and MADDEN, P. A., 1984, *Phys. Rev.* B, **29,** 1035.
[26] PYPER, N. C., 1991, *Adv. Solid State Chem.*, **2,** 223.
[27] WILSON, M., MADDEN, P. A., PYPER, N. C., and HARDING, J. H., 1996, *J. chem. Phys.*, **104,** 8086.
[28] HARDING, J. H., and PYPER, N. C., 1995, *Phil. Mag. Lett.*, **71,** 113.
[29] DICK, B. G., and OVERHAUSER, A. W., 1958, *Phys. Rev.*, **112,** 90.
[30] PYPER, N. C., 1994, *Chem. Phys. Lett.*, **220,** 70.
[31] ROWLEY, A. J., 1998, D.Phil thesis, University of Oxford; ROWLEY, A. J., JEMMER, P., WILSON, M., and MADDEN, P. A., 1998, *J. chem. Phys.*, **108,** 10209.
[32] SANGSTER, M. J. L., and DIXON, M., 1976, *Adv. Phys.*, **23,** 247.
[33] WELLS, A. F., 1984, *Structural Inorganic Chemistry* (Oxford: Clarendon Press).
[34] MÜLLER, U., 1993, *Inorganic Structural Chemistry* (Chichester: Wiley).
[35] WILSON, M., and MADDEN, P. A., 1994, *J. Phys. Condens. Matter*, **6,** 159.
[36] *Handbook of Physics and Chemistry*, 1996 (Boca Raton, FL: CRC Press); STARK, J. G., and WALLACE, H. G., 1984, *Chemistry Data Book* (London: John Murray).
[37] GUNSILIUS, H., BOORMANN, H., SIMON, A., and URLAND, W., 1988, *Z. Naturf.* B, **43,** 1023.
[38] SEARS, V. F., 1992, *Neutron News*, **3,** 26.
[39] AKDENIZ, Z., and TOSI, M. P., 1999, *Z. Naturf.* A, **54,** 477; 1998, *Z. Naturf.*, **53,** 960; *Nuovo Cimento* D, **20,** 1111; AKDENIZ, Z., PASTORE, G., and TOSI, M. P., 1997, *Phys. Chem. Liquids*, **35,** 93.
[40] MADDEN, P. A., and WILSON, M., 2000, *J. Phys. Condens. Matter*, **12,** A95.
[41] WILSON, M., and MADDEN, P. A., 1997, *Molec. Phys.*, **92,** 197; WILSON, M., and RIBEIRO, M. C. C., 1999, *Molec. Phys.*, **96,** 867.
[42] SABOUNGI, M.-L., PRICE, D. L., SCAMEHORN, C., and TOSI, M. P., 1991, *Europhys. Lett.*, **15,** 283.
[43] MOCHINAGA, J., IWADATE, Y., and FUKUSHIMA, K., 1991, *Mater. Sci. Forum*, **73–75,** 147.
[44] WILSON, M., and MADDEN, P. A., 1998, *Phys. Rev. Lett.*, **80,** 532.
[45] HUTCHINSON, F., WILSON, M., and MADDEN, P. A., 2000, *J. Phys: Condens. Matter*, **12,** 10389.